TiO_2-Low Band Gap Semiconductor Heterostructures for Water Treatment Using Sunlight-Driven Photocatalysis

Raquel Del Angel, Juan C. Durán-Álvarez and
Rodolfo Zanella

Additional information is available at the end of the chapter

http://dx.doi.org/10.5772/intechopen.76501

Abstract

Heterogeneous photocatalysis is a promising advanced oxidation process for water purification, given its potential to fully oxidize organic pollutants and to inactivate microorganisms. Due to its versatility and high performance in a broad range of conditions, titanium dioxide (TiO_2)-based photocatalysis has been systematically used at laboratory scale to treat water of different quality. Even though TiO_2 is an exceptional photocatalyst, its broad band gap value (3.2 eV) makes necessary the use of UV light to achieve the photoactivation. This results in the underutilization of the material in sunlight-driven photocatalysis schemes. In order to overcome this handicap, the synthesis of heterostructures using low band gap semiconductors coupled with TiO_2 has brought exceptional materials for visible light-driven photocatalysis. In this chapter, the fundamentals of the synthesis and photoactivation of TiO_2-low band gap semiconductor heterostructures are explored. The mechanisms leading to the increase of the photocatalytic activity of such heterostructures are described. A summary of the available data on the photocatalytic performance of TiO_2-based heterostructures is presented, in terms of degradation of organic pollutants in water using visible light and sunlight. A comparison of the depuration performance of powdered and thin film heterostructures is given at the end of the chapter.

Keywords: composites, heterojunctions, metallic oxides, organic pollutants, semiconductors, water treatment

1. Introduction

Water and wastewater treatment brings new challenges due to the occurrence of new and refractory contaminants produced by anthropogenic activities [1, 2]. In the past few years, water depuration aimed to remove particles, the bulk of organic matter and inactivate microorganisms. However, nowadays, the degradation not only of organic pollutants at trace levels but its precursors and by-products is especially pursued in drinking water treatment systems. For instance, the biological and chemical degradation of fluoroquinolone antibiotics results in the generation of some by-products displaying antibiotic residual activity. Biological and abiotic degradation of personal care products, such as triclosan and triclocarban, leads to the emergence of polychlorinated biphenyls and dioxins. Some bacterial residues in surface water bodies, such as microcystin and geosmin, may impact in the organoleptic properties of drinking water as well as express toxicity, while some iodinated pharmaceuticals may be precursors of trihalomethanes. Under this scenario, the most advanced water treatment systems should aim to completely mineralize the organic pollutants, in order to take the risks of water contamination to the minimum. The complete mineralization of organic pollutants can be warranted by few processes, such as photocatalysis [3–7]. This process is based on the generation of highly reactive $^{\bullet}OH$ radicals, which are able to fully oxidize organic molecules. Heterogeneous photocatalysis process has shown to be efficient in the degradation of organic pollutants in water, avoiding the transport and use of potentially hazardous materials, such as acids or H_2O_2, while the catalyst can be recovered and reused in several cycles [8, 9].

TiO_2 is a widely used semiconductor in heterogeneous photocatalysis due to its high activity and stability [10–12]. This harmless material is currently used not only for water treatment but in food preparation and disinfection of surgical equipment. Anatase is the most photoactive phase of TiO_2, followed by rutile; however, the wide band gap value of both phases (3.0–3.2 eV) results in the activation of these materials under UV-A light irradiation [13]. In order to take the photocatalysis process toward sustainability, it is necessary to develop materials with high photo-response under sunlight irradiation. Given that sunlight comprises only 4–5% of UV-A light, the need to find nanostructures capable to absorb visible light—which composes 50% of the sunlight spectrum [14]—becomes imperative. A growing number of modifications of TiO_2 at nanometric scale have been performed in order to achieve the complete photoactivation of this semiconductor under visible light irradiation. Doping with nonmetal atoms has given partially positive results, since the redshift of the absorption edge of TiO_2 increases in turn the recombination rate of the hole-electron pair. The development of heterostructures based on TiO_2 coupled to low band gap semiconductors could be an efficient approach to improve the photocatalytic conversion of contaminants in water [12, 15, 16]. This chapter explores the fundamentals of the synthesis and photoactivation of the TiO_2-low band gap semiconductor heterostructures, and presents some of the reported data on the photocatalytic activity of these materials, in order to bring light on their potential use for water purification at a higher scale.

2. Fundamentals on the formation and photoexcitation of TiO_2-based heterostructures

A heterostructure or junction is defined as the interfacial union of two or more components. In photocatalysis, heterounions are formed to improve the efficiency of a semiconductor either by redshifting the light absorption or through the decrease of the recombination of the hole-electron pairs [12, 17, 18]. Heterostructures are commonly built up by combining a specific semiconductor with one or more materials, such as metals, semiconductors or organic molecules for example, azo dyes or polymers.

Semiconductor/metal junctions are heterostructures based on the deposition of metallic nanoparticles on crystalline semiconductors. Such union is able to hinder the electron/hole recombination through the sequestration of the photoelectrons from the conduction band of the semiconductor to the surface of the metallic nanoparticles [12] (**Figure 1**). The differences in the Fermi level reached in the semiconductor/metal junction triggers the sequestration of photoelectrons; although other factors, such as the higher work function and electronegativity of the metal, favor the transference of the charge carriers [16, 19, 20]. The defects created in the semiconductor/conductor junction are proposed as the main route of the electron transfer from one material to the other. The Schottky barrier created in the junction impedes the return of the charge carriers to the conduction band of the semiconductor. Typically, low loadings of metallic nanoparticles tend to be the optimal for achieving the highest potential of the electron trap process. However, when this optimal loading is surpassed, the electron traps are converted into charge carriers recombination sites, leading to the dramatic drop of the photocatalytic performance [21–23]. Even when the electron trap effect is unable to significantly redshift the light absorption of the heterostructure, some photocatalytic activity can be achieved by the surface plasmon resonance (SPR) effect, which is expressed by the oscillation of the electrons in the conduction band of the metallic nanoparticles when electromagnetic excitation at a determined wavelength is provided [24–26]. Some extent of photocatalytic activity has been attributed to SPR effect, although this cannot be considered as determinant in the photodegradation of pollutants in water when compared with that achieved under UV light irradiation.

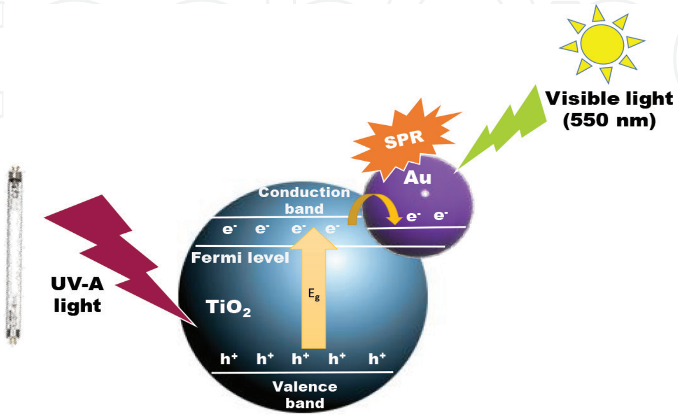

Figure 1. Photoactivation and charge carriers transfer in a semiconductor/conductor heterounion.

The synthesis of semiconductor/semiconductor nanocomposites provides an efficient way to redshift the photoactivation of TiO_2-based materials. When these materials are exposed to visible light, the low band gap semiconductor is activated, producing the hole–electron pair. Then, the photoelectrons migrate from the surface of the low band gap semiconductor to the conduction band of TiO_2, as an effect of the difference in the redox potential between both semiconductors (**Figure 2**). The process leads to the drop of the hole-electron pair recombination rate, resulting in the oxidation process in the low band gap semiconductor, and the reduction process on the TiO_2 surface [17, 27].

When the composite is photoactivated under UV light irradiation, the hole-electron pairs are produced in the highest occupied molecular orbital (HOMO) and the lowest unoccupied molecular orbital (LUMO) of each semiconductor. Charge carriers are then transported and accumulated in the HOMO and LUMO of one of the semiconductors, as a function of gradient in the potential of the bands (**Figure 3**). For this kind of schemes, p-n heterostructures have shown the best results in the separation of the photo-formed charge carriers. However, in some cases, decreasing of the redox potential of charge carriers can occur, depending of

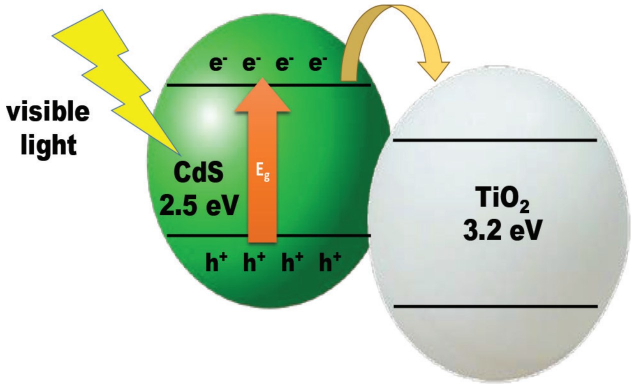

Figure 2. Photoactivation and charge carriers transfer in a TiO_2-low band gap semiconductor heterounion when photoactivation with visible light occurs.

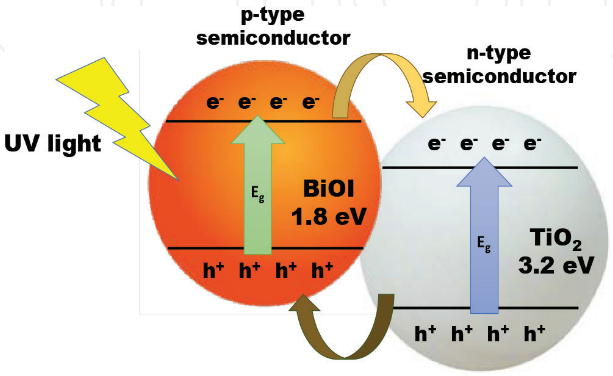

Figure 3. Photoactivation and charge carriers transfer in a TiO_2-low band gap semiconductor heterounion when photoactivation with UV light occurs.

the HOMO and LUMO positions of the semiconductors in the heterostructure, leading to the decrement in the photocatalytic performance [15, 17, 18].

In some advanced approaches, metallic nanoparticles are settled in the heterounion of the two semiconductors. Noble metal nanoparticles can act as electron mediators, transporting the charge carriers from one semiconductor to another, increasing with this the electron trap effect. Heterostructures based on p-n semiconductors have shown a notable increase in the charge separation when noble metal nanoparticles are added in the semiconductor heterounion. These materials, known as all solid-state Z schemes, provide highly reductive photoelectrons and highly oxidative photo-holes by the process shown in **Figure 4** [28].

Photoelectrons are transported from semiconductor II to semiconductor I via the metallic nanoparticles. At the same time, photoelectrons are formed in semiconductor I and photoholes in the HOMO of semiconductor I are recombined with photoelectrons coming from the LUMO of semiconductor II. This kind of schemes impedes the recombination of the charge carriers with the highest oxidative and reductive potential, increasing not only the photocatalytic performance of the components, but bringing chances to photodegrade more recalcitrant pollutants because of the increment of the oxidative potential of the charge carriers.

When TiO_2 nanoparticles are deposited on graphene sheets, the semiconductor/polymer junction displays higher photocatalytic activity due to the transfer of the charge carriers from the semiconductor to the polymer, as shown in **Figure 5b**. Even when the lifetime of the charge carriers is increased, visible light-driven activity is not improved; however, graphene materials can be used as an excellent electron mediator in all solid Z schemes. On the other hand, organic molecules, which are able generate the triplet state under visible light irradiation, can act as sensitizers when deposited on the TiO_2 surface (**Figure 5a**). In this case, electrons are injected from the sensitized molecule to the LUMO of the semiconductor, triggering the photocatalytic process [29].

2.1. Classification of the semiconductors/semiconductor heterostructures

Semiconductor/semiconductor junctions can be classified depending on either the type of semiconductors that are being coupled or by the band structure they present. Considering the type of semiconductors, the semiconductor/semiconductor heterostructures can be classified

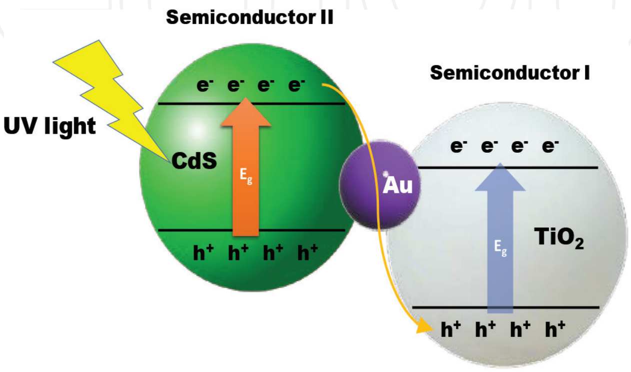

Figure 4. Photoactivation and charge carriers transfer in a TiO_2 based all solid Z scheme when photoactivation when UV light activation occurs.

either as anisotype—a p-n junction—, or isotype heterojunctions, in which both coupled semiconductors are n-type (n-n junction) or p-type (p–p junction). Some examples of n-type semiconductors include TiO_2, WO_3, ZnO, Fe_2O_3, CeO_2, AgI, $BiVO_4$, CdS, CdSe, Bi_2WO_6, and ZnSe, while for p-type semiconductors Bi_2O_3, V_2O_5, BiOI, BiOBr, BiOCl, CuO, Cu_2O can be mentioned [18]. When semiconductor/semiconductor heterostructures are classified depending on the band position of the components, three main groups can be mentioned. **Figure 6** shows the three possible band alignments in semiconductor/semiconductor heterostructures.

In a type I heterostructure, also known as straddling alignment, the band gap value of the semiconductor B is smaller than that of semiconductor A (**Figure 6**). In this case, the potential of valence band of the semiconductor B is located at a higher position than that of semiconductor A, while conduction band of semiconductor A displays a lower potential than that of the conduction band of semiconductor B. In this scheme, electrons and holes are transferred from A to B, resulting in the accumulation of charge carriers in B [18]; this facilitates in turn the recombination of the charge carriers and decreases the photocatalytic activity. Obregon et al. [30] reported the formation of a type I heterojunction using monoclinic $BiVO_4$ and TiO_2. The 1 wt. % m-$BiVO_4$/TiO_2 nanocomposite was prepared by a simple impregnation method and was tested in the degradation of phenol. This system has been tested by other authors using different approaches and modification [31–33]. Other semiconductors that have been coupled to TiO_2 to form a type I heterojunction [18] are WO_3 [34, 35], Fe_2O_3 [36], MoS_2 [37] and BiOI [36].

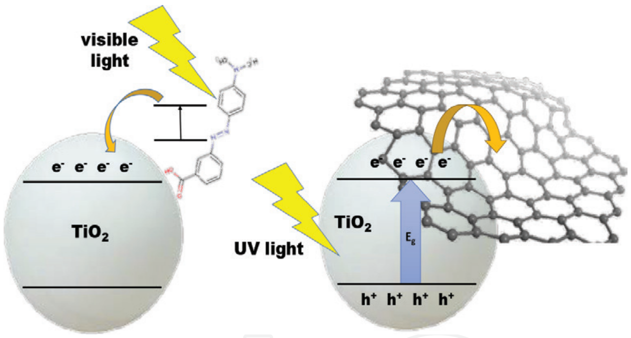

Figure 5. Photoactivation and charge carriers transfer in a TiO_2-sensitized materials under visible light activation (a) and in TiO_2-graphene heterostructures when UV light occurs (b).

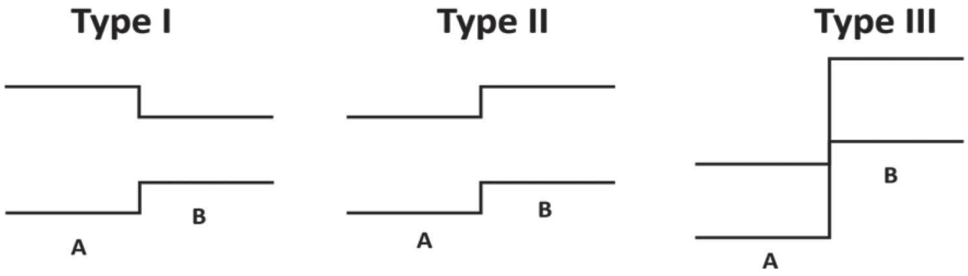

Figure 6. Classification of semiconductor/semiconductor heterostructures based on the band alignment of the components.

Type II heterostructure, or staggered lineup, represents the most efficient configuration for the charge carriers transfer. In this case, photo-generated electrons will be transferred from semiconductor B to semiconductor A, while the holes are moving from semiconductor A to semiconductor B. A more efficient charge separation is achieved, having both photoelectrons and photo-holes distributed in the two semiconductors. A large number of type II heterojunctions have been synthesized with TiO_2, by the union with CdS [38], CdSe [39, 40], Bi_2S_3 [41], WS_2 [42], V_2O_5 [43], Bi_2O_3 [44], CuO [45], Cu_2O [45, 46], and CeO_2 [47].

Type III heterojunctions are similar in structure to the type II composites, but a wider difference in the position of bands between semiconductor A and B is observed. This type of heterojunctions is also known as broke-gap junction, which is highly recommended to the construction of all solid Z schemes. For instance, Heng et al. [48] prepared a type III heterojunction by incorporating $H_3PW_{12}O_{40}$, TiO_2 and In_2S_3. The authors propose that the $H_3PW_{12}O_{40}$ assists in the transfer of electronics from TiO_2 to In_2S_3.

3. Synthesis methods to obtain TiO_2-based heterostructures

A wide variety of physical and chemical methods have been developed for the synthesis of TiO_2-based heterostructures, using a vast diversity of structures and morphologies. Some examples of such methods are sol-gel, solvothermal, impregnation, sputtering, dip-coating, co-precipitation, mechanical synthesis and chemical vapor deposition, among others. In many cases, a combination of two or more synthetic methods and reaction steps are needed in order to create a specific photocatalyst with the desired characteristics. The use of photocatalyst powders for water purification has been of great interest. This is because of the simplicity in the synthesis, the high exposition of the particle surface area to the target pollutants, as well as the high dispersion of the catalyst. In this section, some of the most used methods for the synthesis of TiO_2-based heterostructures are explored.

Sol-gel: The sol-gel method consists of the acidic or basic hydrolysis of an organometallic precursor, followed by a slow polymerization. The obtained material is dried, allowing the decomposition and elimination of all the organic components present in the gel.

WO_3/TiO_2 nanocomposites have been synthesized by the sol-gel method using $Ti(OBu_4)$ and ammonium tungstate as main precursors [35, 49]. The photocatalytic activity of the material was tested via the degradation of malathion using natural sunlight. The complete degradation of the pollutant was achieved after a 2 h irradiation and a mineralization rate of 63% upon 5 h. Yang et al. [47] reported the synthesis of different CeO_2/TiO_2 heterostructures by the sol-gel synthetic route, using $Ti(OBu)_4$ and $Ce(NO_3)_3 \cdot 6H_2O$ as precursors. The synthesized materials were tested for the degradation of methyl orange, noting the enhanced activity of the CeO_2/TiO_2 composite compared with unmodified TiO_2 and CeO_2.

Hydrothermal/solvothermal method: The solvothermal method allows the synthesis of crystalline materials by heating the precursors in solution inside a sealed reactor (autoclave). Water (hydrothermal) and several organic compounds such as ethylene glycol and glycerol (solvothermal) may be used as solvent during the reaction. The solvothermal method is one of the most common preparation techniques for heterostructures, since the variation of pressure and temperature parameters allows the formation of a wide diversity of crystal morphologies. The products obtained are usually well dispersed in form and size. Also, some additives and templates may be added into de reaction mixture to favor a desired morphology or crystallite size. Xu et al. [50] synthesized a rutile/anatase TiO_2 heterostructure using titanium tetrachloride ($TiCl_4$), urea and cetyl trimethyl ammoniumbromide (CTAB) as a template. Reaction was carried out at 160°C for 12 h, resulting in rutile/anatase nanoflowers with high surface area —up to 106.29 m^2/g—. CdS/TiO_2 composites were synthesized by Wu et al. [27] via the microemulsion-mediated solvothermal method, allowing the formation of anatase nanoparticles with highly dispersed CdS nanocrystals on the surface. The modification of TiO_2 with CdS nanoparticles increased the absorption of visible light irradiation at 550 nm. Zhu et al. [51] prepared Bi_2O_3/TiO_2 flower-like spheres, which displayed high photocatalytic activity due to an enhanced visible light absorption. $TiO_2@MoO_3$ core@shell structures were synthesized by Li et al. [52] using a one-step hydrothermal method, while Liu et al. [53] used this method to achieve the formation of a series of $Cu_2O@TiO_2$ core@shell structures by coating different Cu_2O polyhedral nanoparticles on the TiO_2 surface. Cu_2O/TiO_2 hollow spheres (HS) were synthesized by both solvothermal and sol–gel methods [54]. In a first step, TiO_2 HS were synthesized by a sol–gel method, using carbon nanospheres as a template. In the second step, the HS were mixed with a glucose solution, containing $CuSO_4{\cdot}5H_2O$; then, the mixture was poured into a teflon-lined stainless-steel autoclave. In this reaction, glucose took the role of reducing agent, which helped to reduce copper from Cu^{2+} to Cu^{1+}. These heterostructures were tested for the photocatalytic degradation of Rhodamine B under visible and sunlight irradiation, showing promising results.

Impregnation: This method consists of the saturation of one specific support—in this case TiO_2—with a solution containing the desired precursor, usually a metal salt; this allows the metal ions to fill the support pores. Then, the material is dried and exposed to a thermal treatment.

Perales-Martínez et al. [55] reported the formation of the $InVO_4/TiO_2$ catalyst. In a first step, both $InVO_4$ and TiO_2 were prepared using the solvothermal method. Then, the composite was formed by suspending both oxides in methanol in order to achieve the impregnation assisted by ultrasonication. Lastly, the solvent was evaporated using a rotary evaporator. In another work, Maeda et al. [56] reported the formation of cobalt oxide nanoparticles supported on the surface of rutile TiO_2 (Co_3O_4/TiO_2 heterostructure). In this case, TiO_2 was impregnated with the $Co(NO_3)_2{\cdot}6H_2O$ solution, followed by a thermal treatment in air atmosphere. Fe_2O_3/TiO_2 photocatalyst was prepared using a $Fe(NO_3)_3{\cdot}9H_2O$ ethanol solution, where TiO_2 powders were stirred and sonicated [57]. Peng et al. [58] reported that after calcination at 300°C for 6 h, the Fe_2O_3 was deposited on the surface of TiO_2 nanorods. In other report, the preparation of RuO_2/TiO_2 heterostructures was achieved by Uddin et al. [59] using ruthenium(III) pentan-2,4-dionate as RuO_2 precursor.

UV light irradiation: This method consists of the reduction and precipitation of one or more soluble precursors over the surface of TiO_2, which acts as a support. The presence of UV light irradiation allows the photo-formation of electrons in the support, which are responsible of reducing the chemical species in the solution.

MoS_2/TiO_2 and WS_2/TiO_2 have been synthesized by the photo-reduction of either $(NH_4)_2MoS_4$ or $(NH_4)_2WS_4$, directly on the surface TiO_2 particles [42]. These materials showed good efficiency in the degradation of methylene blue and 4-chlorophenol.

Electrosynthesis: The electrosynthesis method consists of the use of electrochemical cells to produce the desired material. Yang et al. [39] achieved the electrodeposition of CdSe nanoparticles on the surface and the inner space of TiO_2 nanotubes (TNTs). For this, three electrodes were used, namely a Pt wire (counter electrode), a saturated calomel electrode (reference electrode) and the TNTs (working electrode). The three electrodes were submerged in an electrolyte solution containing $CdCl_2$ and SeO_2. CdSe was deposited at −0.7 V, −6 V vs. reference electrode at room temperature. Well-dispersed CdSe nanoparticles deposited on TiO_2 were obtained.

Mechanical mixing: This is one of the simplest synthesis methods, which involves the direct mixing of the heterostructure precursors. Manual mixing usually results in long reaction times and low homogeneity of the products. In certain cases, binding agents may be added to the mixture in order to increase the stability of the heterostructure.

Shifu et al. [60] prepared the WO_3/TiO_2 heterostructure using the mechanical mixing method. The precise amounts of TiO_2 and WO_3 powders were mixed in an agate ball milling tank. The two oxides were mixed for 12 h at 300 rpm. A loading of 3% wt. of WO_3 presented the best efficiency for the degradation of monocrotophos. The coupled photocatalyst showed a redshift in its light absorption compared to pure TiO_2.

Precipitation and co-precipitation: Both precipitation and co-precipitation methods consist of the formation of an insoluble material, starting from one or several solutions containing the soluble precursors. Usually, an increase in the pH value of the solution helps in the formation of insoluble hydroxides, allowing the precipitation. Yu et al. [61] prepared an $Ag/AgCl/TiO_2$ heterostructure by the impregnation of TNTs with a 1 M HCl aqueous solution, followed by a second impregnation with a 0.1 M $AgNO_3$ solution. As a result, AgCl nanoparticles were precipitated on the TNTs. Lastly, UV irradiation was applied to achieve a partial reduction of the formed AgCl nanoparticles into metallic Ag.

Thin films: One of the main burdens of using powder photocatalysts is the need of including a separation step for the effluent in order to reuse the photocatalyst in further cycles. This step can become difficult and very expensive, making the photocatalytic process less viable in a plant scale approach. A feasible solution is the immobilization of the material in a suitable support, such as glass, quartz or polymer. Some synthetic routes for obtaining photocatalysts as thin films are described below.

Dip-coating: This is one of the most used methods for the synthesis of thin films, which consists of submerging, at a constant rate, the substrate in a solution containing the precursor of the semiconductor. After a certain dwell time, the substrate is pulled out of the solution. Lastly, the solvent is dried, and a thermal treatment can be applied to eliminate organic residuals and induce crystallization of the semiconductor in the film.

Spin Coating: This process consists of putting a small amount of a solution containing the precursor of the thin film material on the surface of the substrate. Then, the substrate is rotated at high speed, eliminating the excess solution and leaving a uniform film once the solvent is dried.

Sputtering: In this route, ionized atoms (e.g., Ar^+) are accelerated into the surface of a cathodic material. This collision causes that some atoms are ejected from the surface of the electrode.

Subsequently, the ejected atoms are condensed on the surface of the substrate (anode), forming the thin film.

Chemical vapor deposition: This method uses volatile precursors at high temperature. The gaseous species react forming intermediates which are diffused and adsorbed on the surface of the substrate. Further reactions can take place on the surface on the substrate.

4. Photocatalytic activity of TiO_2-based heterostructures under visible and simulated sunlight

The coupling of TiO_2 with low band gap semiconductors leads to the activation of the photocatalyst material under visible light irradiation, as established earlier, resulting in turn in the generation of materials with high efficiency and stability. An important number of studies have reported the photocatalytic performance of these heterostructures, showing high conversion rates of organic and inorganic pollutants in water. Some of these results are shown in **Table 1**. As observed in the table, conversion of azo dyes molecules is the most used way to assess the photocatalytic activity of the synthesized materials. This is due to the easy analytical determination of such molecules in water—most of them for UV–vis spectroscopy—in comparison with uncolored molecules—such as phenols—organochlorinated compounds and pharmaceutical substances. However, as was recently pointed out, using azo dyes molecules in the evaluation of the photocatalytic performance of semiconductors may result in an artifact because of the sensitization of the semiconductors by the adsorbed organic molecules [62]. It is worth noting how the degradation rate constant is mostly determined using the pseudo first-order approach, forgetting the multiple phase conditions. In very few studies, other models—such as the Langmuir-Hinshelwood approximation—have been used [63]. Degradation yields is the most reported parameter in this kind of experiments. Very few studies follow the content of the total organic carbon throughout the process, ignoring with this the mineralization yield of the pollutants. This may lead to a miscalculation of the risk that treated water pose on the exposed organisms, since some of the photodegradation by-products may be more toxic or recalcitrant than the parent compound. Examples of this are benzoquinone, which degradation requires more energy than phenol and triclosan, which degrades into a low toxicity dioxin.

In most cases reported in the literature, halogen lamps are the light sources in photocatalysis schemes, while the loading of the catalyst is maintained below 1 g/L, in order to avoid the screening of light due to the high turbidity in the suspension. Concentration of the organic pollutants is normally set at levels of mg/L, which are one to three magnitude orders higher than those observed in the environment, even in wastewater [1, 64, 65]. The use of such concentration levels enables the determination of the kinetic constants in the photocatalytic degradation of the pollutants in water. However, when experimental conditions require the use of complex liquid matrices, such as superficial water, groundwater or wastewater, the degradation rate is reduced, bringing the opportunity for lowering the initial concentration of the target compound toward environmentally relevant levels, such as μg/L or even ng/L, with no impact in the study of the kinetic constants.

Heterostructure components	Architecture	Pollutant removed	Reaction conditions	Performance	Reference
$FeWO_4/TiO_2$ Fe:Ti ratio = 95:5	Composite	Salicylic acid (6.9 ppm)	300 W Xe lamp ($\lambda \geq 420$ nm). 10 mg of composite were suspended in 50 mL. 120 min of irradiation time.	$k^* = 0.053\ h^{-1}$	[69]
$FeWO_4/TiO_2/CdS$ Fe:Ti:Cd ratio = 5:94:1				$k^* = 0.099\ h^{-1}$	
60 wt. % Cu_2S/TiO_2		Orange II (15 ppm)	150 W tungsten-halogen-lamp with UV cutoff filter at 475 nm. pH ~ 6.4.	$k^* \sim 6.1 \times 10^{-3}\ min^{-1}$	[70]
Bi_2O_3/TiO_2 Bi:Ti molar ratio = 1:100		*p*-chlorophenol (12.88 ppm)	150 W xenon lamp ($\lambda \geq 420$ nm). 0.001 g mL^{-1} of catalyst. 6 h of irradiation time.	Degradation yield of 49%	[71]
TiO_2/Fe_3O_4 (30:70)		Cr(VI) (20 ppm of $K_2Cr_2O_7$)	Mercury vapor lamp of 125 W with a broadband from 250 to 450 nm (maxima at 254, 312 and 365 nm). 30 mg of catalyst in 100 mL of solution.	Complete reduction to Cr(III) in 30 min. $k = 0.91\ ppm\ g^{-1}\ min^{-1}$	[72]
Carbon-doped anatase/brookite TiO_2 (80:20)	Composite	Methylene blue (3.2 ppm)	Solar simulator with filter for blue light. 0.06 g of powder in 100 mL solution. 60 min irradiation.	$k = 0.008\ min^{-1}$	[73]
Rutile/anatase TiO_2	Nanoflowers	Methylene blue (15 ppm)	350 W xenon lamp. 10 mg of catalyst. 120 min of irradiation time.	72% degradation of degradation rate.	[50]
			Adding 0.5 mL of a 30% m/v H_2O_2 solution.	~88% of degradation rate.	

Heterostructure components	Architecture	Pollutant removed	Reaction conditions	Performance	Reference
$BiVO_4$@TiO_2	Core@shell	Methylene blue (5 ppm)	Osram Dulux S67 blue light Bulbs, with maximum emission at 450 nm. 50 mg of the catalyst were dispersed in 150 mL. 120 min irradiation.	~85% of Degradation rate.	[74]
5 wt. % WO_3/TiO_2	Composite	Methyl orange (20 ppm) 2,4-dichlorophenol (20 ppm)	1000 W halogen lamp ($\lambda > 420$ nm). Catalyst loading of 1.1 g L^{-1}. 5 h of time irradiation.	85% degradation 73% degradation	[34]
12 wt. % $Zn_xCd_{1-x}S/TiO_2$ Cd:Zn ratio = 3:1	Composite	Rhodamine B (4.8 ppm)	500 W halogen lamp (420 nm $< \lambda <$ 800 nm). 0.04 g of the catalyst was added to 80 mL of solution. 120 min of irradiation time.	~95% degradation	[75]
Cu_2O/TiO_2	Cu_2O nanospheres decorated with TiO_2 nanoislands.	Methyl Orange (30 ppm)	Light intensity of ~23 mW cm^{-2} ($\lambda > 400$ nm). 0.03 g of catalyst was dispersed in 150 mL of solution. 40 min of irradiation time.	~97% degradation r^{+}~12.825 mg g^{-1} min^{-1}	[76]
Cu_2O@TiO_2	Core@shell Polyhedra (cubes, cuboctahedra and octahedra)	Methylene Blue (3.2 ppm)	300 W xenon lamp with a glass filter ($\lambda > 400$ nm). Light intensity of 23 mW cm^{-2}. Concentration of 0.2 mg photocatalyst mL^{-1}. 4 h of irradiation time.	Up to 80% degradation for octahedra core-shell structure.	[53]
		4-Nitrophenol (10 ppm)	0.02 g of photocatalyst was dispersed in 50 mL of solution.	Up to 50% degradation for octahedra core-shell structure.	

Heterostructure components	Architecture	Pollutant removed	Reaction conditions	Performance	Reference
Bi_2MoO_6/TiO_2 Bi:Ti ratio = 1:2.6	Nanofibers	Rhodamine B (10 ppm)	150 W xenon lamp. 0.1 g of catalyst was suspended in 100 mL of the compound solution. 5 h of irradiation.	92% degradation	[77]
0.5 wt.% $InVO_4/TiO_2$	Composite	Phenol (30 ppm)	300 W lamp with an intensity irradiation of 38.4 W m^{-2}. 0.05 g of catalyst dispersed in 50 mL of solution. 80 min of irradiation time	100% of degradation rate. $k^{\#} = 8.1\times10^{-4}$ s^{-1}	[55]
Polydopamine@TiO_2	Core@shell nanoparticles and brush-like structures.	Geosmin (1000 ppb)	350 W xenon lamp equipped with a 420 nm cutoff filter. 120 min of irradiation	90% degradation	[78]
		Fluorene (1000 ppb)		98% degradation	
Bi_2O_3/TiO_2 Bi:Ti ratio = 10%	Composite	Ofloxacin (25 ppm)	Solar irradiation with average light intensity of 70.3 K lux. Catalyst concentration of 0.5 g/L. 120 min of irradiation time	92.4% degradation	[79]
60 wt. % Sb_2S_3/TiO_2	Nanorods	p-hydroxyazobenzene (10 ppm).	500 W halogen lamp with two cutoff filters (below 420 nm and above 850 nm). 40 mg of catalyst were dispersed in 80 mL. 5 h of irradiation time.	89% of degradation rate	[80]
		Methyl orange		96% of degradation rate	
$Ag/AlO_2/TiO_2$ 90:10 Al:Ti mass ratio	Composite	Formaldehyde (10 ppm)	Sunlight irradiation with an intensity of 90 ± 15 mW/cm^2. 0.1 g of catalyst was dispersed in 100 mL of solution. 90 min of irradiation time.	97.8% of degradation rate	[81]

Heterostructure components	Architecture	Pollutant removed	Reaction conditions	Performance	Reference
Cu_2O/TiO_2	Nanotubes	Rhodamine B (5 ppm)	500 W tungsten halogen lamp with an optical filter ($\lambda > 420$ nm). 120 min of irradiation time.	31% of degradation rate $k^* = 0.00312\ min^{-1}$	[82]
$AgBr/Ag_3PO_4/TiO_2$ Ag:Ti molar ratio = 1:5	Spheres	Methyl orange (8.2 ppm).	Simulated sunlight lamp with intensity of 4 W m^{-2}. 0.001 g of catalyst was dispersed in 6 mL of solution. 50 min of irradiation time.	~90% of degradation rate $k^* = 0.1329\ min^{-1}$	[83]
		Microcystin-LR (50 ppm)	0.01 g of catalyst was dispersed in 30 mL of solution.	100% of degradation after 5 min. $k^* = 0.6371\ min^{-1}$	
7 wt. % $Fe_2O_3@TiO_2$	Core@shell	Rhodamine B (10 ppm)	350 W xenon lamp. 5 mg of catalyst were dispersed in 50 mL of aqueous solution. 5 h of irradiation time.	60% of degradation rate $k^* = 0.1605\ h^{-1}$	[84]
Cu_2O/TiO_2	Octadecahedron/ Quantum Dot	Methyl orange (30 ppm)	500 W xenon lamp with glass filter ($\lambda > 400$ nm) and intensity of 100 mW cm^{-2}. 25 mg of catalyst were dispersed in 100 mL of solution. 60 min of irradiation.	97% of degradation rate $k^* = 0.055\ min^{-1}$	[85]
$BiOBr/TiO_2$ molar ratio Ti:Bi = 2:1	Nanorods	Rhodamine B (15 ppm)	300 W Xenon lamp with a cut-off glass filter ($\lambda > 420$ nm). Illumination intensity of 7×10^3 mW cm^{-2}. 70 mg of photocatalyst were dispersed in 70 mL of solution.	99.9% of degradation after 10 min of irradiation. $k = 0.49\ min^{-1}$ 88.5% mineralization.	[86]
		Cr (VI) (50 ppm $K_2Cr_2O_7$ solution)		95.4% of conversion after 120 min irradiation. $k = 0.025\ min^{-1}$	

Heterostructure components	Architecture	Pollutant removed	Reaction conditions	Performance	Reference
Cu_2O/TiO_2	Nanoparticles/ nanotubes	p-nitrophenol (20 ppm)	Xe lamp ($\lambda > 420$ nm). with an intensity of 100 mW cm^{-2}. 210 min of irradiation.	35–40% of degradation rate under visible light irradiation. >90% of degradation rate under sunlight irradiation.	[87]
Bi_2S_3/TiO_2	Fungus-like mesoporous Bi_2S_3/TiO_2 nanotube	2,4-dichlorophenoxyacetic acid (2,4-D) (10 ppm)	Xenon lamp with a radiation intensity of 85 mW cm^{-2}. 180 min of irradiation time.	71% degradation ~75% mineralization (after 360 min of irradiation)	[41]
		2,4-D and Cr(VI) (10 ppm)		81% degradation for 2,4-D Complete Cr(VI) reduction.	
Cu_2O/TiO_2	Hollow spheres	Rhodamine B (5 ppm)	300 W xenon lamp. 0.1 g of catalyst was dispersed in 200 mL of the compound solution. 120 min irradiation time	~ 88% of degradation rate. $k^* = 0.0165$ min^{-1}	[54]
			300 W Xenon lamp with a 420 nm cut off filter. 300 min time irradiation.	~ 92% of degradation rate. $k^* = 0.0081$ min^{-1}	
1 wt. % Ag_2CO_3/TiO_2	Composite	Methyl orange (20 ppm)	300 W iodine tungsten lamp. 0.05 g of catalyst was suspended in 80 mL of the compound solution. 5 h of irradiation time.	~75% degradation $k^* = 0.24$ min^{-1}	[88]

*Degradation rate constants approximated to the pseudo first-order kinetics.

+Reaction rate (degradation rate).

#Kinetic constants of photodegradation estimated by the Langmuir-Hinshelwood model according to a first-order reaction.

Table 1. Degradation performance using TiO_2-based heterostructures under different experimental conditions.

Even when for the results shown in **Table 1**, direct comparisons are difficult to be established, it seems clear that tailored heterostructures formed by TiO_2 and low band gap semiconductors are efficient to achieve high photocatalytic degradation yields under visible light irradiation when azo dyes are used as target pollutants. For most of the reported heterostructures, degradation yields above 80% were obtained; except for the Cu_2O/TiO_2 material, which performance was as low as 31%. On the other hand, very low photocatalytic efficiency is observed for refractory industrial pollutants, such as nitrophenols and chlorophenols. These compounds displayed degradation yields lower than 50% when Cu_2O-TiO_2 and Bi_2O_3/TiO_2 heterostructures were used in photocatalytic assays under visible light irradiation. Some environmentally relevant pollutants, which are commonly found in surface water sources, are efficiently removed by the visible light-driven photocatalysis process. A high concentration of microcystin, a toxin produced by cyanobacteria, is fully degraded in 5 min under visible light irradiation, when $AgBr/Ag_3PO_4/TiO_2$ nanospheres are used as photocatalyst, while 90% of degradation of environmentally relevant concentrations of geosmin was achieved upon 120 min using core@shell polydopamine@TiO_2 composites. Also, high loads of pharmaceutically active substances, bisfenol A and the widely used herbicide 2,4-D are efficiently removed from water under visible light by the TiO_2 based heterostructures. From these results, the use of these materials in advanced oxidation processes for ternary drinking water treatment sounds like a plausible option, keeping in mind that the high efficiency showed in these lab-scale studies can be affected by the complexity of the liquid matrix. Regarding heavy metals, the complete photocatalytic reduction of hexavalent chromium has been reported using Fe_2O_3/TiO_2 and Bi_2S_3/TiO_2 heterostructures in a very short time lapse, while BiOBr-based composites showed a slightly lower activity. For the studies reported in **Table 1**, the occurrence of synergistic effects was observed when the photocatalytic performance of the heterostructures and their single components was compared. For some cases, the increment in the degradation rate and degradation yields was found in the order of 1.5–5 fold, demonstrating that the efficiency of the heterostructure was significantly higher than the sum of the performance of the single components.

When the photocatalytic performance of thin films is assessed, a clear decrease in the degradation rate of organic pollutants is observed. This is because of the decrease in the number of active sites exposed to the aqueous matrix due to the immobilization of the photocatalyst on a substrate. Degradation rates as low as 30% in 15 h for of azo dyes have been reported using TiO_2-$InVO_4$ thin films [66], although the efficiency can be improved by the deposition of noble metal nanoparticles on the film surface. Conversely, in other study [67], the complete degradation of methyl orange was achieved in 8 h of visible light irradiation by using BiOCl-TiO_2 thin films. This study reveals the importance of the charge carrier transference in the immobilized photocatalyst material. When this factor is taken into account, the reactivity of the thin film surface increases, leading to a higher photocatalytic activity and overcoming the mass transference hindrance.

In this sense, the arrangement of the heterostructure components is of high relevance since some approaches may favor the transfer of photo-holes or photoelectrons to the surface of the thin films. In this sense, Monfort et al. [68] tested the transfer of charge carriers in the $BiVO_4$-TiO_2 heterostructure, noting the occurrence of oxidation reactions by photo-holes when $BiVO_4$ was located on the surface of the thin films, while reduction reactions given by photoelectron were prominent when TiO_2 was in contact with the aqueous matrix.

5. Conclusions

Even when TiO_2 displays an outstanding performance as photocatalyst, its limitation to absorb light and photoactivate under visible light irradiation makes necessary to develop a set of strategies to overcome this handicap. Coupling of low band gap semiconductors with TiO_2 nanoparticles is an auspicious approach not only to redshift the light absorption of the composite, but to reduce the recombination rate of the hole-electron pair by the transference of the charge carriers from one semiconductor to another, increasing the photocatalytic performance. This leads to the generation of materials with high photoactivity and stability under visible light and sunlight irradiation.

In order to obtain functional heterostructures, care must be taken in the selection of the composite components, in order to get the best alignment of the semiconductors bands and thus the optimal transference of the charge carriers from one component to the other. Type II and III heterostructures have shown the highest efficiency in the separation of the hole-electron pairs. The defects formed in the heterounion act as transference sites for the charge carriers; although it only works when tiny loadings of semiconductor particles are deposited on TiO_2, and recombination centers appear in the heterounion when the optimal loading is surpassed. The p-n heterostructures, specially the all solid Z schemes, have shown not only the efficient separation of the charge carriers in the composite, but the generation of highly oxidant photo-holes, which opens the opportunity to photodegrade highly recalcitrant organic pollutants in water. To date, very few TiO_2-based Z schemes have been explored; thus, investigation should aim to develop new schemes, beyond the TiO_2-Au-CdS approach, using nontoxic semiconductors, such as BiOI, ZnS, Ag_2O or graphene.

TiO_2-based heterostructures have shown a notable high performance in the photocatalytic removal of organic and inorganic pollutants in water under visible light irradiation. In some cases, removal yields surpass those observed for the individual components of the heterostructure, indicating the occurrence of a synergistic effect. New challenges are in the development of functional heterostructures in the form of thin films, which will optimize the energy and space consumption in photocatalytic water treatment systems.

The photocatalysis processes have the potential to move toward sustainability, through the development of sunlight active heterostructures, which simultaneously perform the oxidation of organic pollutants and the reduction of water molecule for hydrogen generation. This will lead to energy autonomous treatment systems based on sunlight-driven photocatalysis. Lastly, investigations should aim to the development of green synthesis methods, which optimize the energy consumption and minimize the use of harmful reagents.

Acknowledgements

The authors want to than to Secretaria de Ciencia, Tecnología e Innovación de la Ciudad de México and Dirección General de Asuntos del Personal Académico de la UNAM for the financial supporting given to this work through projects SECITI/047/2016 and IA101916, respectively.

Author details

Raquel Del Angel, Juan C. Durán-Álvarez* and Rodolfo Zanella

*Address all correspondence to: carlos.duran@ccadet.unam.mx

Institute of Applied Science and Technology, National Autonomous University of Mexico, Mexico City, Mexico

References

[1] Richardson SD, Ternes TA. Water analysis: Emerging contaminants and current issues. Analytical Chemistry. 2014;**86**:2813-2848. DOI: 10.1021/ac500508t

[2] Murray KE, Thomas SM, Bodour AA. Prioritizing research for trace pollutants and emerging contaminants in the freshwater environment. Environmental Pollution. 2010;**158**:3462-3471. DOI: 10.1016/j.envpol.2010.08.009

[3] Oller I, Malato S, Sánchez-Pérez JA. Combination of advanced oxidation processes and biological treatments for wastewater decontamination–A review. Science of the Total Environment. 2011;**409**:4141-4166. DOI: 10.1016/j.scitotenv.2010.08.061

[4] Andreozzi R, Vincenzo C, Insola A, Marotta R. Advanced oxidation processes (AOP) for water purification and recovery. Catalysis Today. 1999;**53**:51-59. DOI: 10.1016/S0920-5861(99)00102-9

[5] Matilainen A, Sillanpää M. Removal of natural organic matter from drinking water by advanced oxidation processes. Chemosphere. 2010;**80**:351-365. DOI: 10.1016/j.chemosphere.2010.04.067

[6] Klavarioti M, Mantzavinos D, Kassinos D. Removal of residual pharmaceuticals from aqueous systems by advanced oxidation processes. Environment International. 2009;**35**: 402-417. DOI: 10.1016/j.envint.2008.07.009

[7] Deng Y, Zhao R. Advanced oxidation processes (AOPs) in wastewater treatment. Current Pollution Reports. 2015;**1**:167-176. DOI: 10.1007/s40726-015-0015-z

[8] Padmanaban VC, Giri Nandagopal MS, Madhangi Priyadharshini G, Maheswari N, Janani Sree G, Selvaraju N. Advanced approach for degradation of recalcitrant by nanophotocatalysis using nanocomposites and their future perspectives. International Journal of Environmental Science and Technology. 2016;**13**:1591-1606. DOI: 10.1007/s13762-016-1000-9

[9] Hoffmann MR, Martin S, Choi W, Bahnemann DW. Environmental applications of semiconductor photocatalysis. Chemical Reviews. 1995;**95**:69-96. DOI: 10.1021/cr00033a004

[10] Kumar SG, Rao KSRK. Comparison of modification strategies towards enhanced charge carrier separation and photocatalytic degradation activity of metal oxide semiconductors (TiO_2, WO_3 and ZnO). Applied Surface Science. 2017;**391**:124-148. DOI: 10.1016/j.apsusc.2016.07.081

[11] Fagan R, McCormack DE, Dionysiou DD, Pillai SC. A review of solar and visible light active TiO_2 photocatalysis for treating bacteria, cyanotoxins and contaminants of emerging concern. Materials Science in Semiconductor Processing. 2016;**42**:2-14. DOI: 10.1016/j.mssp.2015.07.052

[12] Linsebigler AL, Lu G, Yates JT. Photocatalysis on TiO_2 surfaces: Principles, mechanisms, and selected results. Chemical Reviews. 1995;**95**:735-758

[13] Sclafani A, Herrmann JM. Comparison of the photoelectronic and photocatalytic activities of various anatase and rutile forms of titania in pure liquid organic phases and in aqueous solutions. The Journal of Physical Chemistry. 1996;**100**:13655-13661. DOI: 10.1021/jp9533584

[14] Priecel P, Adekunle Salami H, Padilla RH, Zhong Z, Lopez-Sanchez JA. Anisotropic gold nanoparticles: Preparation and applications in catalysis. Chinese Journal of Catalysis. 2016;**37**:1619-1650. DOI: 10.1016/S1872-2067(16)62475-0

[15] Daghrir R, Drogui P, Robert D. Modified TiO_2 for environmental photocatalytic applications: A review. Industrial and Engineering Chemistry Research. 2013;**52**:3581-3599. DOI: 10.1021/ie303468t

[16] Park H, Park Y, Kim W, Choi W. Surface modification of TiO_2 photocatalyst for environmental applications. Journal of Photochemistry and Photobiology C: Photochemistry Reviews. 2013:1-20. DOI: 10.1016/j.jphotochemrev.2012.10.001

[17] Kumar SG, Devi LG. Review on modified TiO_2 photocatalysis under UV/visible light: Selected results and related mechanisms on interfacial charge carrier transfer dynamics. Journal of Physical Chemistry A. 2011;**115**:13211-13241. DOI: 10.1021/jp204364a

[18] Marschall R. Semiconductor composites: Strategies for enhancing charge carrier separation to improve photocatalytic activity. Advanced Functional Materials. 2014;**24**:2421-2440. DOI: 10.1002/adfm.201303214

[19] Zhang Z, Yates JT. Band bending in semiconductors: Chemical and physical consequences at surfaces and interfaces. Chemical Reviews. 2012;**112**:5520-5551. DOI: 10.1021/cr3000626

[20] Primo A, Corma A, García H. Titania supported gold nanoparticles as photocatalyst. Physical Chemistry Chemical Physics. 2011;**13**:886-910. DOI: 10.1039/C0CP00917B

[21] Zhang X, Chen YL, Liu R-S, Tsai DP. Plasmonic photocatalysis. Reports on Progress in Physics. 2013;**76**:46401. DOI: 10.1088/0034-4885/76/4/046401

[22] Jovic V, Chen WT, Sun-Waterhouse D, Blackford MG, Idriss H, Waterhouse GIN. Effect of gold loading and TiO_2 support composition on the activity of Au/TiO_2 photocatalysts for H_2 production from ethanol-water mixtures. Journal of Catalysis. 2013;**305**:307-317. DOI: 10.1016/j.jcat.2013.05.031

[23] Bowker M, James D, Stone P, Bennett R, Perkins N, Millard L, Greaves J, Dickinson A. Catalysis at the metal-support interface: Exemplified by the photocatalytic reforming

of methanol on Pd/TiO_2. Journal of Catalysis. 2003;**217**:427-433. DOI: 10.1016/S0021-9517(03)00074-5

[24] Eustis S, El-Sayed MA. Why gold nanoparticles are more precious than pretty gold: Noble metal surface plasmon resonance and its enhancement of the radiative and non-radiative properties of nanocrystals of different shapes. Chemical Society Reviews. 2006;**35**:209-217. DOI: 10.1039/B514191E

[25] Zhou X, Liu G, Yu J, Fan W. Surface plasmon resonance-mediated photocatalysis by noble metal-based composites under visible light. Journal of Materials Chemistry. 2012;**22**:21337. DOI: 10.1039/c2jm31902k

[26] Kamat PV. Photophysical, photochemical and photocatalytic aspects of metal nanoparticles. Journal of Physical Chemistry B. 2002;**106**:7729-7744. DOI: 10.1021/jp0209289

[27] Wu L, Yu JC, Fu X. Characterization and photocatalytic mechanism of nanosized CdS coupled TiO_2 nanocrystals under visible light irradiation. Journal of Molecular Catalysis A: Chemical. 2006;**244**:25-32. DOI: 10.1016/j.molcata.2005.08.047

[28] Zhou P, Yu J, Jaroniec M. All-solid-state Z-scheme photocatalytic systems. Advanced Materials. 2014;**26**:4920-4935. DOI: 10.1002/adma.201400288

[29] Li X, Yu J, Wageh S, Al-Ghamdi AA, Xie J. Graphene in photocatalysis: A review. Small. 2016:1-57. DOI: 10.1002/smll.201600382

[30] Obregón S, Colón G. A ternary Er^{3+}-$BiVO_4$/TiO_2 complex heterostructure with excellent photocatalytic performance. RSC Advances. 2014;**4**:6920-6926. DOI: 10.1039/c3ra46603e

[31] Hu Y, Li D, Zheng Y, Chen W, He Y, Shao Y, Fu X, Xiao G. $BiVO_4$/TiO_2 nanocrystalline heterostructure: A wide spectrum responsive photocatalyst towards the highly efficient decomposition of gaseous benzene. Applied Catalysis B: Environmental. 2011;**104**:30-36. DOI: 10.1016/j.apcatb.2011.02.031

[32] Zhang L, Tan G, Wei S, Ren H, Xia A, Luo Y. Microwave hydrothermal synthesis and photocatalytic properties of TiO_2/$BiVO_4$ composite photocatalysts. Ceramics International. 2013;**39**:8597-8604. DOI: 10.1016/j.ceramint.2013.03.106

[33] Pingmuang K, Chen J, Kangwansupamonkon W, Wallace GG, Phanichphant S, Nattestad A. Composite photocatalysts containing $BiVO_4$ for degradation of cationic dyes. Scientific Reports. 2017;**7**:1-11. DOI: 10.1038/s41598-017-09514-5

[34] Leghari SAK, Sajjad S, Chen F, Zhang J. WO_3/TiO_2 composite with morphology change via hydrothermal template-free route as an efficient visible light photocatalyst. Chemical Engineering Journal. 2011;**166**:906-915. DOI: 10.1016/j.cej.2010.11.065

[35] Ramos-Delgado NA, Hinojosa-Reyes L, Guzman-Mar IL, Gracia-Pinilla MA, Hernández-Ramírez A. Synthesis by sol-gel of WO_3/TiO_2 for solar photocatalytic degradation of malathion pesticide. Catalysis Today. 2013;**209**:35-40. DOI: 10.1016/j.cattod.2012.11.011

[36] Mou F, Xu L, Ma H, Guan J, Chen D, Wang S. Facile preparation of magnetic γ-Fe_2O_3/TiO_2 Janus hollow bowls with efficient visible-light photocatalytic activities by asymmetric shrinkage. Nanoscale. 2012;**4**:4650-4657. DOI: 10.1039/c2nr30733b

[37] Zhou W, Yin Z, Du Y, Huang X, Zeng Z, Fan Z, Liu H, Wang J, Zhang H. Synthesis of few-layer MoS_2 nanosheet-coated TiO_2 nanobelt heterostructures for enhanced photocatalytic activities. Small. 2013;**9**:140-147. DOI: 10.1002/smll.201201161

[38] Serpone N, Borgarello E, Grätzel M. Visible light induced generation of hydrogen from H_2S in mixed semiconductor dispersions; improved efficiency through interparticle electron transfer. Journal of the Chemical Society, Chemical Communications. 1984;**6**:342-344. DOI: 10.1039/C39840000342

[39] Yang L, Luo S, Liu R, Cai Q, Xiao Y, Liu S, Su F, Wen L. Fabrication of CdSe nanoparticles sensitized long TiO_2 nanotube arrays for photocatalytic degradation of anthracene-9-carbonxylic acid under green monochromatic light. Journal of Physical Chemistry C. 2010;**114**:4783-4789. DOI: 10.1021/jp910489h

[40] Toyoda T, Yindeesuk W, Kamiyama K, Katayama K, Kobayashi H, Hayase S, Shen Q. The electronic structure and photoinduced electron transfer rate of CdSe quantum dots on single crystal rutile TiO_2: Dependence on the crystal orientation of the substrate. The Journal of Physical Chemistry C. 2016;**120**:2047-2057. DOI: 10.1021/acs.jpcc.5b09528

[41] Yang L, Sun W, Luo S, Luo Y. White fungus-like mesoporous Bi_2S_3 ball/TiO_2 heterojunction with high photocatalytic efficiency in purifying 2,4-dichlorophenoxyacetic acid/Cr(VI) contaminated water. Applied Catalysis B: Environmental. 2014;**156-157**:25-34. DOI: 10.1016/j.apcatb.2014.02.044

[42] Ho W, Yu JC, Lin J, Yu J, Li P. Preparation and photocatalytic behavior of MoS_2 and WS_2 nanocluster sensitized TiO_2. Langmuir. 2004;**20**:5865-5869. DOI: 10.1021/la049838g

[43] Jianhua L, Rong Y, Songmei L. Preparation and characterization of the TiO_2-V_2O_5 photocatalyst with visible-light activity. Rare Metals. 2006;**25**:636-642

[44] Yang J, Dai J, Li J. Visible-light-induced photocatalytic reduction of Cr(VI) with coupled Bi_2O_3/TiO_2 photocatalyst and the synergistic bisphenol A oxidation. Environmental Science and Pollution Research. 2013;**20**:2435-2447. DOI: 10.1007/s11356-012-1131-6

[45] Helaïli N, Bessekhouad Y, Bouguelia A, Trari M. Visible light degradation of Orange II using xCu_yO_z/TiO_2 heterojunctions. Journal of Hazardous Materials. 2009;**168**:484-492. DOI: 10.1016/j.jhazmat.2009.02.066

[46] Bessekhouad Y, Robert D, Weber J-V. Photocatalytic activity of Cu_2O/TiO_2, Bi_2O_3/TiO_2 and $ZnMn_2O_4$/TiO_2 heterojunctions. Catalysis Today. 2005;**101**:315-321. DOI: 10.1016/j.cattod.2005.03.038

[47] Yang H, Zhang K, Shi R, Tang A. Sol-gel synthesis and photocatalytic activity of CeO_2/TiO_2 nanocomposites. Journal of the American Ceramic Society. 2007;**90**:1370-1374. DOI: 10.1111/j.1551-2916.2007.01540.x

[48] Heng H, Gan Q, Meng P, Liu X. The visible-light-driven type III heterojunction $H_3PW_{12}O_{40}/TiO_2$-In_2S_3: A photocatalysis composite with enhanced photocatalytic activity. Journal of Alloys and Compounds. 2017;**696**:51-59. DOI: 10.1016/j.jallcom.2016.11.116

[49] Yang H, Shi R, Zhang K, Hu Y, Tang A, Li X. Synthesis of WO_3/TiO_2 nanocomposites via sol-gel method. Journal of Alloys and Compounds. 2005;**398**:200-202. DOI: 10.1016/j.jallcom.2005.02.002

[50] Xu H, Li G, Zhu G, Zhu K, Jin S. Enhanced photocatalytic degradation of rutile/anatase TiO_2 heterojunction nanoflowers. Catalysis Communications. 2015;**62**:52-56. DOI: 10.1016/j.catcom.2015.01.001

[51] Zhu J, Wang S, Wang J, Zhang D, Li H. Highly active and durable Bi_2O_3/TiO_2 visible photocatalyst in flower-like spheres with surface-enriched Bi_2O_3 quantum dots. Applied Catalysis B: Environmental. 2011;**102**:120-125. DOI: 10.1016/j.apcatb.2010.11.032

[52] Li N, Li Y, Li W, Ji S, Jin P. One-step hydrothermal synthesis of TiO_2@MoO_3 Core-Shell nanomaterial: Microstructure, growth mechanism, and improved photochromic property. Journal of Physical Chemistry C. 2016;**120**:3341-3349. DOI: 10.1021/acs.jpcc.5b10752

[53] Liu L, Yang W, Sun W, Li Q, Shang JK. Creation of Cu_2O@TiO_2 composite photocatalysts with p—N heterojunctions formed on exposed Cu_2O facets, their energy band alignment study, and their enhanced photocatalytic activity under illumination with visible light. ACS Applied Materials and Interfaces. 2015;**7**:1465-1476. DOI: 10.1021/am505861c

[54] Yin H, Wang X, Wang L, Nie Q, Zhang Y, Wu W. Cu_2O/TiO_2 heterostructured hollow sphere with enhanced visible light photocatalytic activity. Materials Research Bulletin. 2015;**72**:176-183. DOI: 10.1016/j.materresbull.2015.07.030

[55] Perales-Martínez IA, Rodríguez-González V, Lee SW, Obregón S. Facile synthesis of $InVO_4/TiO_2$ heterojunction photocatalysts with enhanced photocatalytic properties under UV-vis irradiation. Journal of Photochemistry and Photobiology A: Chemistry. 2015;**299**:152-158. DOI: 10.1016/j.jphotochem.2014.11.021

[56] Maeda K, Ishimaki K, Okazaki M, Kanazawa T, Lu D, Nozawa S, Kato H, Kakihana M. Cobalt oxide nanoclusters on rutile titania as bifunctional units for water oxidation catalysis and visible light absorption: Understanding the structure-sctivity relationship. ACS Applied Materials and Interfaces. 2017;**9**:6114-6122. DOI: 10.1021/acsami.6b15804

[57] Zhou W, Fu H, Pan K, Tian C, Qu Y, Lu P, Sun C-C. Mesoporous TiO_2/α-Fe_2O_3: Bifunctional composites for effective elimination of arsenite contamination through simultaneous photocatalytic oxidation and adsorption. Journal of Physical Chemistry C. 2008;**112**:19584-19589. DOI: 10.1021/jp806594m

[58] Peng L, Xie T, Lu Y, Fan H, Wang D. Synthesis, photoelectric properties and photocatalytic activity of the Fe_2O_3/TiO_2 heterogeneous photocatalysts. Physical Chemistry Chemical Physics. 2010;**12**:8033-8041. DOI: 10.1039/c002460k

[59] Uddin MT, Babot O, Thomas L, Olivier C, Redaelli M, D'Arienzo M, Morazzoni F, Jaegermann W, Rockstroh N, Junge H, Toupance T. New insights into the photocatalytic properties of RuO_2/TiO_2 mesoporous heterostructures for hydrogen production and

organic pollutant photodecomposition. Journal of Physical Chemistry C. 2015;**119**:7006-7015. DOI: 10.1021/jp512769u

[60] Shifu C, Lei C, Shen G, Gengyu C. The preparation of coupled WO_3/TiO_2 photocatalyst by ball milling. Powder Technology. USA. 2005;**160**:198-202. DOI: 10.1016/j.powtec.2005.08.012

[61] Yu J, Dai G, Huang B. Fabrication and characterization of visible-light-driven plasmonic photocatalyst $Ag/AgCl/TiO_2$ nanotube arrays. The Journal of Physical Chemistry C. 2009;**113**:16394-16401. DOI: 10.1021/jp905247j

[62] Barbero N, Vione D. Why dyes should not be used to test the photocatalytic activity of semiconductor oxides. Environmental Science and Technology. 2016;**50**:2130-2131. DOI: 10.1021/acs.est.6b00213

[63] Emeline AV, Ryabchuk VK, Serpone N. Dogmas and misconceptions in heterogeneous photocatalysis. Some enlightened reflections. Journal of Physical Chemistry B. 2005;**109**:18515-18521. DOI: 10.1021/jp0523367

[64] Reemtsma T, Jekel M. Organic Pollutants in the Water Cycle : Properties, Occurrence, Analysis and Environmental Relevance of Polar Compounds. Wiley-VCH; 2006

[65] Miège C, Choubert JM, Ribeiro L, Eusèbe M, Coquery M. Fate of pharmaceuticals and personal care products in wastewater treatment plants—Conception of a database and first results. Environmental Pollution. 2009;**157**:1721-1726. DOI: 10.1016/j.envpol.2008.11.045

[66] Ge L, Xu M, Fang H. Synthesis and characterization of the $Pd/InVO_4$-TiO_2 co-doped thin films with visible light photocatalytic activities. Applied Surface Science. 2006;**253**:2257-2263. DOI: 10.1016/j.apsusc.2006.04.023

[67] Yang J, Wang X, Lv X, Xu X, Mi Y, Zhao J. Preparation and photocatalytic activity of BiO_X-TiO_2 composite films (X=Cl, Br, I). Ceramics International. 2014;**40**:8607-8611. DOI: 10.1016/j.ceramint.2014.01.077

[68] Monfort O, Roch T, Gregor M, Satrapinskyy L, Raptis D, Lianos P, Plesch G. Photooxidative properties of various $BiVO_4/TiO_2$ layered composite films and study of their photocatalytic mechanism in pollutant degradation. Journal of Environmental Chemical Engineering. 2017;**5**:5143-5149. DOI: 10.1016/j.jece.2017.09.050

[69] Bera S, Rawal SB, Kim HJ, Lee WI. Novel coupled structures of $FeWO_4$ /TiO_2 and $FeWO_4$/TiO_2/CdS designed for highly efficient visible-light photocatalysis. Applied Materials & Interfaces. 2014;**6**:9654-9663. DOI: 10.1021/am502079x

[70] Bessekhouad Y, Brahimi R, Hamdini F, Trari M. Cu_2S/TiO_2 heterojunction applied to visible light Orange II degradation. Journal of Photochemistry and Photobiology A: Chemistry. 2012;**248**:15-23. DOI: 10.1016/j.jphotochem.2012.08.013

[71] Bian Z, Zhu J, Wang S, Cao Y, Qian X, Li H. Self-assembly of active Bi_2O_3/TiO_2 visible photocatalyst with ordered mesoporous structure and highly crystallized anatase. Journal of Physical Chemistry C. 2008;**112**:6258-6262. DOI: 10.1021/jp800324t

[72] Challagulla S, Nagarjuna R, Ganesan R, Roy S. Acrylate-based polymerizable sol-gel synthesis of magnetically recoverable TiO_2 supported Fe_3O_4 for Cr(VI) photoreduction in aerobic atmosphere. ACS Sustainable Chemistry & Engineering. 2016;**4**:974-982. DOI: 10.1021/acssuschemeng.5b01055

[73] Etacheri V, Michlits G, Seery MK, Hinder SJ, Pillai SC. A highly efficient $TiO_{2-x}C_x$ nano-heterojunction photocatalyst for visible light induced antibacterial applications. ACS Applied Materials & Interfaces. 2013;**5**:1663-1672. DOI: 10.1021/am302676a

[74] Kontic R, Patzke GR. Synthetic trends for $BiVO_4$ photocatalysts: Molybdenum substitution vs. TiO_2 and SnO_2 heterojunctions. Journal of Solid State Chemistry. 2012;**189**:38-48. DOI: 10.1016/j.jssc.2011.11.050

[75] Li W, Li D, Meng S, Chen W, Fu X, Shao Y. Novel approach to enhance photosensitized degradation of rhodamine B under visible light irradiation by the $Zn_xCd_{1-x}S/TiO_2$ nanocomposites. Environmental Science and Technology. 2011;**45**:2987-2993. DOI: 10.1021/es103041f

[76] Liu L, Yang W, Li Q, Gao S, Shang JK. Synthesis of Cu_2O nanospheres decorated with TiO_2 nanoislands, their enhanced photoactivity and stability under visible light illumination, and their post-illumination catalytic memory. ACS Applied Materials and Interfaces. 2014;**6**:5629-5639. DOI: 10.1021/am500131b

[77] Zhang M, Shao C, Mu J, Zhang Z, Guo Z, Zhang P, Liu Y. One-dimensional Bi_2MoO_6/TiO_2 hierarchical heterostructures with enhanced photocatalytic activity. Crystal Engineering Communication. 2012;**14**:605-612. DOI: 10.1039/C1CE05974B

[78] Liu S, Hu Q, Qiu J, Wang F, Lin W, Zhu F, Wei C, Zhou N, Ouyang G. Enhanced photocatalytic degradation of environmental pollutants under visible irradiation by a composite coating. Environmental Science and Technology. 2017;**51**:5137-5145. DOI: 10.1021/acs.est.7b00350

[79] Sood S, Mehta SK, Sinha ASK, Kansal SK. Bi_2O_3/TiO_2 heterostructures: Synthesis, characterization and their application in solar light mediated photocatalyzed degradation of an antibiotic, ofloxacin. Chemical Engineering Journal. 2016;**290**:45-52. DOI: 10.1016/j.cej.2016.01.017

[80] Sun M, Chen G, Zhang Y, Wei Q, Ma Z, Du B. Efficient degradation of azo dyes over $Sb2S_3/TiO_2$ heterojunction under visible light irradiation. Industrial & Engineering Chemistry Research. 2012;**51**:2897-2903. DOI: 10.1021/ie2025882

[81] Tang A, Jia Y, Zhang S, Yu Q, Zhang X. Synthesis, characterization and photocatalysis of $AgAlO_2/TiO_2$ heterojunction with sunlight irradiation. Catalysis Communications. 2014;**50**:1-4. DOI: 10.1016/j.catcom.2014.02.015

[82] Wang M, Sun L, Lin Z, Cai J, Xie K, Lin C. p–n Heterojunction photoelectrodes composed of Cu_2O-loaded TiO_2 nanotube arrays with enhanced photoelectrochemical and photoelectrocatalytic activities. Energy & Environmental Science. 2013;**6**:1211-1220. DOI: 10.1039/c3ee24162a

[83] Wang X, Utsumi M, Yang Y, Li D, Zhao Y, Zhang Z, Feng C, Sugiura N, Cheng JJ. Degradation of microcystin-LR by highly efficient AgBr/Ag_3PO_4/TiO_2 heterojunction photocatalyst under simulated solar light irradiation. Applied Surface Science. 2015;**325**:1-12. DOI: 10.1016/j.apsusc.2014.10.078

[84] Xia Y, Yin L. Core–shell structured α-Fe_2O_3@TiO_2 nanocomposites with improved photocatalytic activity in the visible light region. Physical Chemistry Chemical Physics. 2013;**15**:18627-18634. DOI: 10.1039/c3cp53178c

[85] Xu X, Gao Z, Cui Z, Liang Y, Li Z, Zhu S, Yang X, Ma J. Synthesis of Cu_2O octadecahedron/TiO_2 quantum dot heterojunctions with high visible light photocatalytic activity and high stability. ACS Applied Materials & Interfaces. 2016;**8**:91-101. DOI: 10.1021/acsami.5b06536

[86] Xue C, Zhang T, Ding S, Wei J, Yang G. Anchoring tailored low-index faceted BiOBr nanoplates onto TiO_2 nanorods to enhance the stability and visible-light-driven catalytic activity. ACS Applied Materials and Interfaces. 2017;**9**:16091-16102. DOI: 10.1021/acsami.7b00433

[87] Yang L, Luo S, Li Y, Xiao Y, Kang Q, Cai Q. High efficient photocatalytic degradation of p-nitrophenol on a unique Cu_2O/TiO_2 p-n heterojunction network catalyst. Environmental Science and Technology. 2010;**44**:7641-7646. DOI: 10.1021/es101711k

[88] Yu C, Wei L, Chen J, Xie Y, Zhou W, Fan Q. Enhancing the photocatalytic performance of commercial TiO_2 crystals by coupling with trace narrow-band-gap Ag_2CO_3. Industrial and Engineering Chemistry Research. 2014;**53**:5759-5766. DOI: 10.1021/ie404283d

IntechOpen